Optimizing the giant magnetoresistance of NiFe/Cu/Co pseudo spin-valves prepared by magnetron sputtering

Amitesh Paul,[a] Thorsten Damm, Daniel E. Bürgler, Simon Stein, Hermann Kohlstedt, and Peter Grünberg
Institut für Festkörperforschung, Forschungszentrum Jülich GmbH, D-52425 Jülich, Germany

(Received 3 December 2002; accepted 31 January 2003)

We study the dependence of magnetic and magnetotransport properties of NiFe/Cu/Co pseudo spin-valves on the pressure of the Ar sputtering gas during magnetron deposition. The giant magnetoresistance (GMR) ratio as a function of the sputtering pressure behaves nonmonotonically with a maximum of about 4% at an intermediate pressure of 0.87×10^{-2} mbar. Magneto-optic Kerr-effect measurements reveal different coercive fields and independent switching of the Co and NiFe layers. The structural characterization by x-ray scattering shows no significant pressure dependence. However, we observe by atomic force microscopy a variation of the grain structure with increasing sputtering pressure; the grain size first decreases and then the grains start clustering for highest pressures. The reduced coercive field and the lower GMR ratio indicate that the clustered grains have weaker magnetic pinning and increased spin-independent scattering. © *2003 American Institute of Physics.* [DOI: 10.1063/1.1563056]

Giant magnetoresistance (GMR) in spin-valves based on different magnetic materials with different coercive fields—so-called pseudo spin-valves—are interesting from the application point of view for developing magnetic sensors and magnetoresistive random access memory technologies.[1] Structures consisting of magnetic layers separated by a nonmagnetic spacer (e.g., Cu) are well known for large GMR ratios at room temperature (RT) and high sensitivity; that is, large change of the resistance at small magnetic fields. The principle involved is rather simple as one magnetic layer, the soft layer, switches at a smaller external field than the so-called hard layer, which gives rise to magnetic antialignment and a change of the spin-dependent scattering rates,[2,3] resulting in change of the resistance.

There have been various attempts to optimize NiFe/Cu/Co pseudo spin-valves by increasing the difference in magnetic coercivity of the two magnetic layers[4,5] or by changing the layer thicknesses.[6] Recently, the influence of the sputtering gas pressure during rf sputtering of the hard CoFe layer in NiFe/Cu/CoFe pseudo spin-valves has been studied.[7] The increase of the GMR ratio with pressure was associated with a small decrease of the grain cluster size.[7]

Thin film nucleation and formation is, apart from temperature, dependent on kinetic energy and the chemical free energy of the atoms arriving at the substrate. In the case of sputtering, the latter parameters sensitively depend on the plasma formed between the source and target. In particular, the grain cluster size depends on these parameters which in turn influences the magnetotransport properties of spin-valves. Due to the magnetic confinement of the plasma in magnetron sputtering, the dependence of plasma properties such as the ionization efficiency on pressure is different from that of rf sputtering.[8] Thus, the effect of changing the sputtering pressure may also be quite different in the case of magnetron sputtering compared to rf sputtering. Therefore in the present study, an attempt has been made to optimize the GMR ratio on NiFe/Cu/Co pseudo spin-valves by changing the sputtering pressure of a magnetron sputtering system. In contrast to Ref. 7, the Ar pressure is the same for all three layers that constitute a particular pseudo spin-valve.

The pseudo spin-valves studied in the present work are structures of NiFe/Cu/Co prepared by dc magnetron sputtering. A base pressure of 1×10^{-7} mbar is achieved by turbomolecular pumps. Samples are prepared by serial deposition of NiFe, Cu, and Co layers onto SiO_2 substrates kept at RT. The sputtering pressure was controlled by the flow of 99.9999% Ar in the chamber. Trilayer samples labeled S1, S2, and S3 of the structure SiO_2/NiFe (5.0 nm)/Cu (3.0 nm)/Co (3.0 nm) are prepared at three different Ar pressures, as listed in Table I. The variations of the sputtering rates (0.037–0.056 nm/s) at different pressures are taken into account to ensure similar thicknesses of the individual layers in all samples. In particular, the Cu spacer thickness does not vary such that the magnetic layers are always decoupled.

X-ray reflectivity (XRR) as well as diffuse x-ray scattering (XDS) measurements[9,10] to characterize the microstructure of the samples are performed using a Bruker-axs D8 diffractometer with Cu K_α radiation. MR are done in specular geometry (angle of incidence Θ_i equal to the angle of reflection Θ_r). Diffuse scattering as a function of the in-plane component of the momentum transfer vector q_x is measured by keeping the scattering angle 2Θ fixed, while rocking the specimen around $\Theta_i=\Theta_r$. MR is measured at RT by the conventional four-probe dc technique, and magnetization loops are recorded by means of the magneto-optic Kerr (MOKE) effect at RT. The magnetic field is applied in the plane of the sample for all measurements. Atomic force microscopy (AFM) measurements are performed in tapping mode using a multimode SPM from Digital Instruments.

Figure 1(a) shows the XRR data of the specimens prepared at different sputtering gas pressure together with their fits. The specular reflectivity spectra are fitted using Parratt's formalism[11] with the following variables: (i) the individual layer thicknesses and (ii) the average rms interface roughness

[a]Author to whom correspondence should be addressed; electronic mail: A.Paul@fz-juelich.de

TABLE I. The GMR ratio, saturation resistance R_s, average feature size, and surface roughness σ_{surface} of spin-valves S1, S2, and S3 prepared at different Ar pressures. The GMR ratio is defined as $(R_0-R_s)/R_s$, where R_s and R_0 are the resistance with and without saturating magnetic field, respectively.

Sample	Ar pressure (10^{-2} mbar)	GMR (%)	R_s (Ω)	Feature size (nm)	σ_{surface} (nm)
S1	0.34	2.5	0.139	180	1.3
S2	0.87	4.0	0.012	78	0.3
S3	1.70	1.3	0.116	229	2.0

$\sigma_{\text{interface}}$. We find that the layer thicknesses indeed are the same for all samples and that there is no significant variation of the interface roughness with pressure, $\sigma_{\text{interface}}=(0.45\pm0.05)$ nm. The diffuse scattering measurements provide information about the in-plane structure of the interfaces, which can be described in terms of the height–height correlation function

$$C(R):=\frac{1}{2\pi A}\int_0^{2\pi} d\vartheta \int_A d^2\rho z(\vec{\rho})z(\vec{\rho}+\vec{\mathrm{R}}), \tag{1}$$

where $\vec{\mathrm{R}}=(R,\vartheta)$ is an in-plane vector in the integration area A, and $z(\vec{\mathrm{R}})$ the height profile. In XRR analysis, $C(R)$ is often parameterized in the form

$$C(R)=\sigma_{\text{interface}}{}^2 \exp\left[-\left(\frac{|R|}{\xi}\right)^{2h}\right], \tag{2}$$

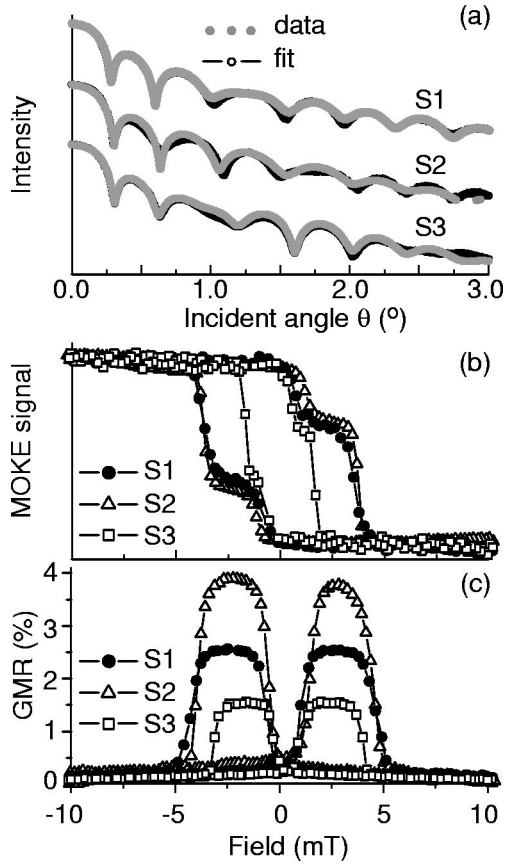

FIG. 1. (a) Specular XRR scans, (b) MOKE hysteresis loops, and (c) MR for spin-valves S1, S2, and S3 prepared at different Ar pressure. The curves in (a) are vertically shifted for the sake of clarity.

where ξ is the in-plane correlation length, and h is the fractal dimension that describes the jaggedness of the interface.[9] We use the model of Ming *et al.*[12] to fit the XDS data, and obtain $\xi=(300\pm20)$ nm and $h=0.5\pm0.2$. There is no significant variation with pressure.

Figure 1(b) shows the MOKE data of the samples. Two distinct separate hysteresis loops corresponding to NiFe (smaller coercivity) and Co (larger coercivity) are seen for the low sputtering pressures, that is, for S1 and S2. Only a weak, but still well-defined separation is seen for highest gas pressure, that is, for S3. The almost equal vertical position of the plateau due to antialignment for all three samples indicates that the fraction of the sample with antiparallel alignment (or the degree of antiparallel alignment) is constant. The corresponding MR curves are plotted in Fig. 1(c). The reduced coercivity of S3 is here reflected by a narrower field range of the high-resistance state. Note, that the GMR ratio for S2 is higher than that of S1 and S3. Thus, the GMR ratio shows a nonmonotonic dependence on the sputtering pressure. This behavior correlates with the different topographies visible in the AFM micrographs in Fig. 2. The lower parts show the height–height correlation function $C(R)$ of the surface profiles, from which we determine the typical size of the surface features. Evenly distributed grains of 180 and 78 nm are observed for S1 and S2, respectively. For S3, however, we observe a different surface morphology with larger congeries or clusters of small grains with an average size of 229 nm and voids in between. Note, that the vertical range for Fig. 2(c) is 4 times larger than for Fig. 2(b). The variation of σ_{surface} [determined from Eq. (2) using $C(0)=\sigma^2_{\text{surface}}$] supports the topological changes from large and small grains in Figs. 2(a) and 2(b), respectively, to an arrangement of grain clusters in Fig. 2(c). These changes do not affect the structural parameters determined from x-ray scattering, probably because these are dominated by the SiO_2/NiFe interface that yields the highest contrast. On the other hand, the volume sensitive saturation resistances R_s clearly reflect the structural differences. R_s of sample S2 is about one order of magnitude smaller than those of samples S1 and S3. The dependence of the GMR ratio, dc saturation resistance (R_s), average feature size (from AFM), and rms surface roughness (σ_{surface} from AFM) on the Ar pressure are summarized in Table I.

In 1974, an electron microscopy study of thick ($\approx\mu$m), sputtered layers of various metals (Cu, Fe, etc.) by Thornton[13] has revealed grain structure dependence on various factors such as the substrate temperature, deposition rates, Ar pressure, and thickness of the layers. Thus, in the present case, there is a wide range of possibilities for the varying grain structure formation as a function of the Ar pressure.

The deposition rates used in our study (0.037–0.056 nm/s) are one order of magnitude lower than usually reported,[7,13] and the substrate heat load is low. The temperature is not expected to increase significantly above RT or to vary with Ar pressure. The slight decrease of the deposition rates with increasing Ar pressure, while all other parameters are kept constant is due to the accumulation of charged particles near the target caused by magnetic confinement and due to more collisions between the ejected particles and the

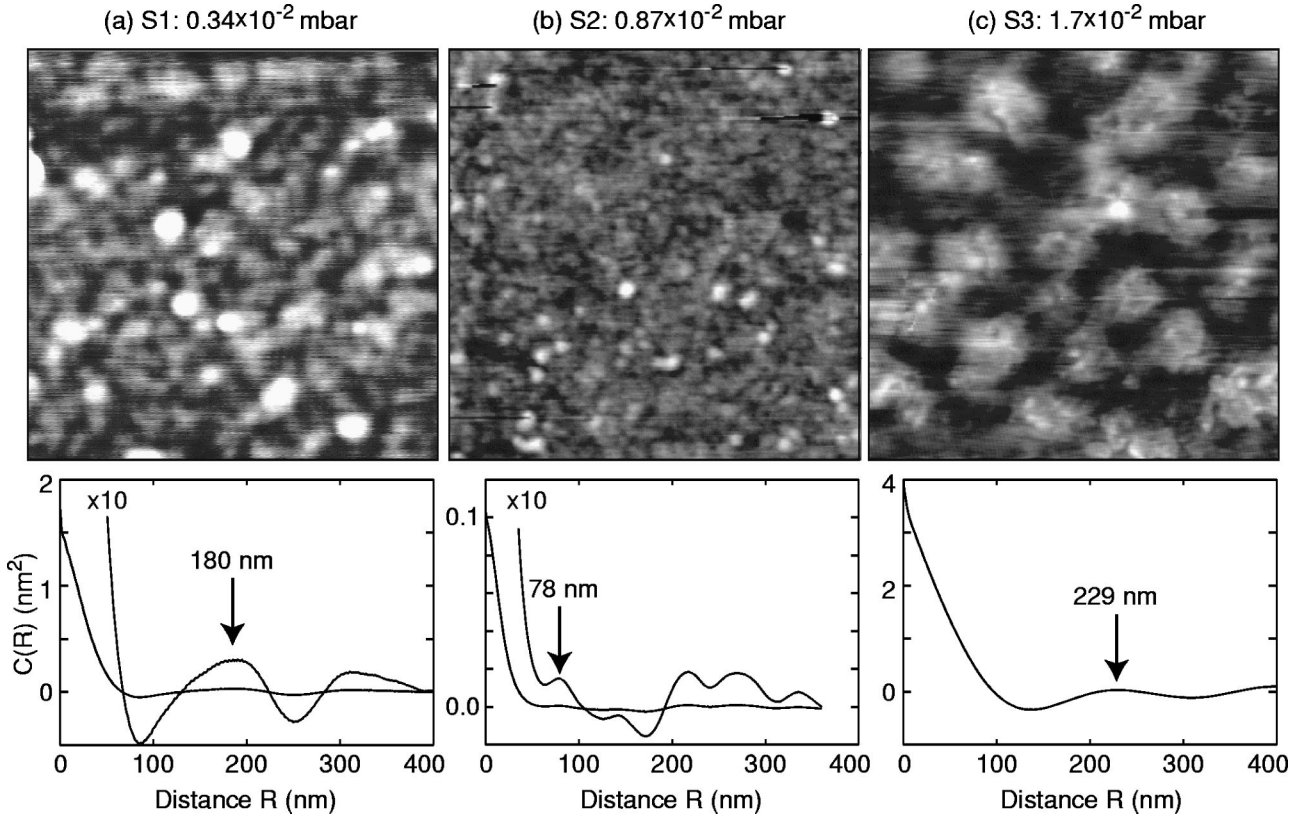

FIG. 2. 1 μm$\times$1 μm AFM micrographs and height–height correlation functions $C(R)$ calculated according to the definition in Eq. (1) from the images of spin-valves (a) S1 (gray-scale range 5.0 nm), (b) S2 (gray scale range 2.5 nm), and (c) S3 (gray scale range 10.0 nm). Arrows mark the first correlation maxima which yield a measure for the typical lateral feature size. Gray curves in (a) and (b) are vertically magnified by a factor of 10.

Ar gas. The mean free path varies in the pressure range from 0.34 to 1.70×10^{-2} mbar between about 3 and 0.5 cm[14] and is always smaller than the target–substrate separation of 6 cm. The pressure increase results in a lower average energy and a broader angular distribution of the particles arriving at the substrate.[13] The reduced energy leads to less surface mobility of the deposited adatoms and a higher nucleation density. Therefore, the grain size decreases with pressure and the grain density increases. This behavior is clearly observed for samples S1 and S2 in Figs. 2(a) and 2(b). The broadening of the angular distribution eventually leads to intergrain shading,[13] which gives rise to a morphology with hillocks or clusters and voids on a length scale larger than the grain size. We relate the undulated topography of sample S3 in Fig. 2(c) to this intergrain shading effect. The smooth surface of the depicted hillocks indicates that they consist of small grains. Both effects—reduction of grain size and intergrain shadowing—are possibly assisted by an increasing amount of absorbed Ar atoms at higher pressure.[13] The clusters in Fig. 2(c) might be the precursor for the formation of the open columnar structures observed at comparable low deposition rates and similar Ar pressure for thicker films.[13,15] The increase in R_s by almost one order of magnitude for highest and lowest pressures (Table I) supports the described structural changes with voids or high-resistive boundaries between large grains for S1 and between grain clusters for S3. Intergrain magnetic interactions within grain clusters of the NiFe and Co layers may cause incoherent magnetic reversal rotation[16] of the clusters, which explains the lower coercivity for sample S3 [Fig. 1(b)].

In conclusion, the GMR ratio of NiFe/Cu/Co pseudo spin-valves prepared by dc magnetron sputtering has been optimized using an intermediate Ar pressure. The nonmonotonic dependence of the GMR ratio on Ar pressure results from (i) the grain size variation and (ii) the onset of grain cluster formation due the intergrain shading. Both effects have an influence on the spin-independent scattering rate as reflected by variations of the saturation resistance.

This work is supported by the HGF-Strategiefonds-project "Magnetoelectronics."

[1] C. Dupas, P. Beauvillain, C. Chappert, J. P. Renard, F. Trigui, P. Veillet, E. Vélu, and D. Renard, J. Appl. Phys. **67**, 5680 (1990).
[2] B. Dieny, V. S. Speriosu, S. S. P. Parkin, B. A. Gurney, D. R. Wilhoit, and D. Mauri, Phys. Rev. B **43**, 1297 (1991).
[3] A. Fert, J. Magn. Magn. Mater. **104–107**, 1712 (1991).
[4] H.-J. Kim, B.-I. Lee, and S.-K. Joo, J. Appl. Phys. **81**, 3995 (1997).
[5] W. Wulfhekel, S. Knappmann, and H. P. Oepen, J. Appl. Phys. **79**, 988 (1996).
[6] D. Lottis, A. Fert, R. Morel, L. G. Pereira, J. C. Jacquet, P. Galtier, J. M. Coutellier, and T. Valet, J. Appl. Phys. **73**, 5515 (1993).
[7] S. Bae, J. Li, J. H. Judy, and S. Zurn, Appl. Phys. Lett. **77**, 3435 (2000).
[8] T. E. Sheridan, M. J. Goeckner, and J. Goree, Appl. Phys. Lett. **57**, 2080 (1990).
[9] T. Salditt, T. H. Metzger, and J. Peisl, Phys. Rev. Lett. **73**, 2228 (1994).
[10] A. Paul and G. S. Lodha, Phys. Rev. B **65**, 245416 (2002).
[11] L. G. Parratt, Phys. Rev. **95**, 359 (1954).
[12] Z. H. Ming, A. Krol, Y. L. Soo, Y. H. Kao, J. S. Park, and K. L. Wang, Phys. Rev. B **47**, 16373 (1993).
[13] J. A. Thornton, J. Vac. Sci. Technol. **11**, 666 (1974).
[14] *Handbook of Chemistry and Physics*, edited by R. C. Weast (CRC Press, Cleveland, 1974); J. A. Thornton, J. Vac. Sci. Technol. **11**, 666 (1974).
[15] C. T. Wu, Thin Solid Films **64**, 103 (1979).
[16] R. W. Vook, Int. Met. Rev. **27**, 209 (1982).